Exp Brain Res (2006) 170: 513–521
DOI 10.1007/s00221-005-0234-4

RESEARCH ARTICLE

**Frederick J. P. Langheim · Alexander N. Merkle
Arthur C. Leuthold · Scott M. Lewis
Apostolos P. Georgopoulos**

Dipole analysis of magnetoencephalographic data during continuous shape copying

Received: 4 February 2005 / Accepted: 26 September 2005 / Published online: 23 November 2005

Abstract High density, whole head magnetoencephalography (MEG) was used to study ten healthy human subjects (five females and five males) participating in a continuous shape-copying task. The task was performed with eyes open and fixated. The three-part task began with 45 s of fixation on a blue dot, after which the dot turned red, and a pentagon was presented around it. Subjects continued to fixate on the red dot for 45 s, after which it turned green. The green dot instructed subjects to begin copying the shape continuously for 45 s, without visual feedback, using a joystick mounted at arm's length. Data were collected at 1,017.25 Hz with a 248 sensor axial-gradiometer system. After cardiac artifact subtraction (Leuthold 2003), each corner was identified, and 1 s epochs (centered on each corner) were averaged and filtered from 1 to 44 Hz. Grand average flux maps demonstrated dipolar distributions identifying the most relevant sensors. With these sensors, which were located over flux extrema (Valaki et al. 2004), dipole models were used for source localization within subjects. Consistent dipole locations included the left motor cortex, bilateral parietal, frontal and temporal regions, and the occipital cortex. These results indicate that MEG source-localization may be derived from a limited number of trials of continuous data, and that visual cortex activity may be consistently present during continuous motor activity despite the absence of novel visual stimulation and eye-movements.

Keywords Magnetoencephalography · MEG · Copying · Vision · Motor

F. J. P. Langheim (✉) · A. N. Merkle · A. C. Leuthold
S. M. Lewis · A. P. Georgopoulos
Brain Sciences Center, Veterans Affairs Medical Center,
One Veterans Drive, Minneapolis, MN 55417, USA
E-mail: frederick.langheim@gmail.com
Tel.: +1-612-7252282
Fax: +1-612-7252291

F. J. P. Langheim · A. N. Merkle · A. C. Leuthold
S. M. Lewis · A. P. Georgopoulos
The Domenici Research Center for Mental Illness,
Veterans Affairs Medical Center, Minneapolis, MN 55417, USA

F. J. P. Langheim · A. C. Leuthold · A. P. Georgopoulos
Department of Neuroscience, University of Minnesota
Medical School, Minneapolis, MN 55455, USA

F. J. P. Langheim · A. P. Georgopoulos
MD/PhD Program, University of Minnesota
Medical School, Minneapolis, MN 55455, USA

S. M. Lewis · A. P. Georgopoulos
Department of Neurology, University of Minnesota
Medical School, Minneapolis, MN 55455, USA

A. P. Georgopoulos
Department of Psychiatry, University of Minnesota
Medical School, Minneapolis, MN 55455, USA

A. P. Georgopoulos
Center for Cognitive Sciences, University of Minnesota,
Minneapolis, MN 55455, USA

Introduction

Traditional magnetoencephalography (MEG) source-localization paradigms involve the averaging of multiple short window stimulus response pairs. Because natural movements evolve in time, this experimental design could limit MEG studies of motor function. Therefore, we sought to explore the feasibility of using a continuous motor task for MEG source-localization. To that end, we chose to use a shape-copying task that has been extensively studied in our laboratory with single-unit recordings in monkeys (Averbeck et al. 2002, 2003) and fMRI in human subjects (Lewis et al. 2003). In this task, subjects were provided with a visual template that they copied using a joystick mounted outside their visual field. Subjects received no visual feedback of the joystick trajectory.

In order to copy a figure, a subject must convert a visual display into a closely approximated motor program. Unlike tracing, in which the motor output corresponds in space with the template, in copying subjects

must transfer visual information about the object being copied to a new space in which the copy is being created. For this more complicated task, subjects must produce and execute a motor plan with the same spatial characteristics as the object being copied, in a "motor field." Bernstein first described this motor field in comparison to the visual field, stating that the motor field emphasizes topology rather than metrics (Bernstein 1923). Georgopoulos (2002) reevaluated recently Bernstein's incisive insight within the context of modern studies of the neural mechanisms of spatial aspects of movement. The topological emphasis is demonstrated by the similarity of an individual's handwriting across letter sizes and orientation of the writing surface, on horizontal paper versus a vertical dry-erase board, for example. The similarity in handwriting holds despite the large differences in muscle groups used to produce it. If specialized cortical regions subserve the motor field, damage to those areas would interfere with specific forms of movement.

Deficits in motor planning or spatial transformation, in the presence of normal vision and normal motor control, may result in the inability to complete a visuoconstructional task such as shape copying. This deficit in assembling, building or drawing components of a model or template into a whole is known as constructional apraxia (Kleist 1934). While Kleist did not differentiate among forms of constructional apraxia, the work of Benton suggested that deficits in shape copying may segregate from stick-construction and block-arranging deficits in a clinical setting (Benton 1967). Furthermore, deficits in drawing from a template can be separate from the ability to draw a similar object from memory (Behrmann et al. 1992).

Shape copying without visual feedback requires identification of the object (or at least its component parts and their relations to one another), motor planning, and an abstract spatial representation that functions to compare the observed figure to the movement being made for copying it. Given these aspects, shape copying is a routine component in neurological assessment (Folstein et al. 1975). As such, shape copying also proves to be a useful task in the study of movement and normal brain function (Averbeck et al. 2002, 2003; Lewis et al. 2003).

Materials and methods

Subjects

Ten right-handed subjects (five women and five men) participated in these experiments as paid volunteers (age range, 23–41 years; mean ± SD, 30 ± 6 years). The study protocol was approved by the appropriate institutional review boards. Informed consent was obtained from all subjects according to the Declaration of Helsinki. All subjects denied any history of neurological or psychiatric illness, including drug/alcohol abuse. In addition, no subjects were found to have abnormal neurological magnetic resonance imaging (MRI) studies.

The copy task

Stimuli were generated by a computer and presented to the subjects using a LCD projector. Subjects performed three 45 s tasks in consecutive order (Lewis et al. 2003). In the first task, they fixated a blue spot of light in the center of a black screen; in the second task, the light changed to red and a single white shape of a pentagon appeared around it; in the third task, the light changed to green (a "go" signal) and the subjects drew the shape continuously by moving an X–Y joystick with their right hand. Subjects were instructed to fixate during all tasks and to draw in the third task. They were also instructed to copy the shapes counterclockwise at their own speed, beginning at top and center; no visual feedback was provided. The fixation point and pentagon were presented to the subjects using a periscopic mirror system which placed the image on a screen approximately 62 cm in front of the subject's eyes. The pentagon subtended approximately 10° of visual angle.

Data acquisition

Data were collected using a 248-channel axial gradiometer MEG system (Magnes 3600 WH, 4D-Neuroimaging, San Diego, CA, USA). The MEG sensor array was located within an electromagnetically shielded room to reduce environmental noise. To monitor unwanted subject motion, five signal coils were digitized prior to MEG acquisition and consecutively activated before and after data acquisition, thereby locating the head in relation to the sensors. The three fiducial locations of the left and right peri-auricular points (center of external acoustic meatus, bilaterally) as well as the nasion (the skin over where the nasal bone joins the skull) were also digitized. Subject motion was no greater than 8 mm, and averaged 3.4 mm across all subjects and tasks. Scalp and fiducial digitization was carried out with a 3-D digitizer (Fastrak 3SF0002, Polhemus Navigator Sciences, Colchester, VT, USA). MEG data were acquired at 1,017.25 Hz and filtered down to 0.1–400 Hz during acquisition. The X–Y output of the joystick was sampled at the same rate as the MEG data (at 1,017.25 Hz) and was incorporated directly into the MEG data file to ensure correct time alignment. Eye movements and eyeblinks were monitored using three electrodes placed around the right eye of each subject; they were located: (1) immediately lateral and superior to the supraorbital notch, (2) at the lateral canthus, and (3) over the center of the inferior orbital rim. The resulting Electrooculogram (EOG) was sampled at 1,017.25 Hz.

In addition to MEG data, anatomical MRI scans were acquired for each subject. In order to insure high quality studies for localization, surface rendering, and

segmentation, these data were acquired at high resolution on a 1.5 T Signa Horizons LX system (GE, Milwaukee, WI, USA) using a neuro-vascular head coil. The volume imaged extended from above the head to below the cerebellum and included the external auditory meatus of each ear. This full head acquisition was necessary for future coregistration, and was acquired as T1 weighted images using a 3-D SPGR sequence (TR = 20 ms, TE = minfull, Flip angle = 30°, FOV = 240×240 mm, slice thickness/gap = 1.4/0, matrix = 256×256, NEX = 1). The resulting voxel resolution was 0.94×0.94×1.5 mm^3. In order to maintain proper left and right orientation for coregistration between MEG and MRI data, MRI studies were performed with a vitamin E tablet taped to the subject's right cheek.

Pre-processing

The acquired MEG data were time series consisting of ~45,000 values per task, subject, and sensor. The magnetic signal from contracting cardiac muscle (cardiac artifact) was removed from each series using event-synchronous subtraction (Leuthold 2003). This method identifies each QRS complex of the cardiac artifact waveform infiltrating the most susceptible MEG sensors. Each Q through U heartbeat is then averaged throughout the acquisition within every individual sensor channel. In turn, the averaged heartbeat artifact, particular to a given sensor, is subtracted from each appearance of the heartbeat artifact within the respective sensor, effectively removing the cardiac artifact from the time series.

Dipole analysis

After cardiac correction, MEG data, *X* and *Y* joystick coordinates, EOG channel information, and head localization files were converted and imported for use in BESA (Brain Electrical Source Analysis software package, version 5.0.4, MEGIS Software GmbH, Gräfelfing, Germany). Unlike the electrocardiogram, which has a relatively uniform MEG tracing, eye-movement artifacts in MEG are quite variable, and depend upon both duration and direction of movement. Therefore, removal of saccade artifacts was not possible using a similar approach as that applied to the cardiac artifact, and eye-blinks and saccades identified in the EOG were marked as artifacts for their duration, excluding those data from averaging. Pentagon sides were identified as illustrated in Fig. 1.

Each one of the five repeated and recognizable corners of the pentagon copies was identified in the *X* and *Y* recordings of each subject (Fig. 1). This allowed for a global average of all corners. The first iteration of the pentagon copy was left out of averaging. Epochs were defined from −500 to +500 ms from the time-point identified as a corner. Whereas individual subjects tended to draw at different speeds, the rate at which a single subject drew repeated copies of the pentagon showed little variation in speed or trajectory. This might have been anticipated from the motor field literature (Bernstein in Whiting 1984). Indeed, it was this limited variation across iterations within each individual that allowed us to create our averaged data sets. However, subjects occasionally did stray from their established pentagon patterns. Interestingly, these variations were

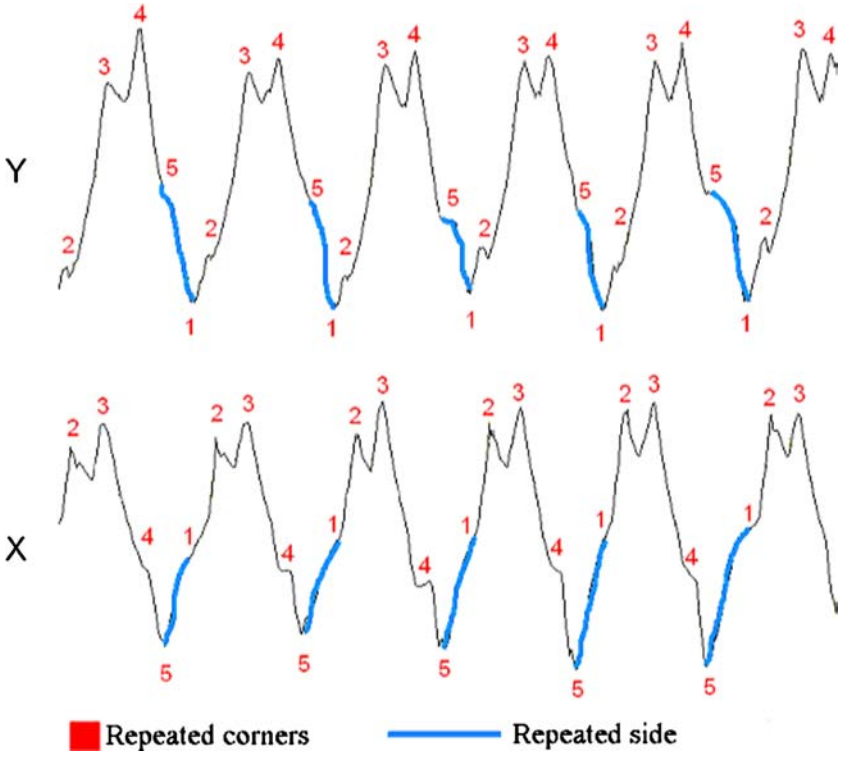

Fig. 1 Partial *X* and *Y* trajectory tracings used to identify corners and sides of each iteration of a copied pentagon. *Red numbers* indicate corners beginning with one at top center and continuing counterclockwise. *Blue lines* indicate the repeated side connecting the fifth and first corners. *X*-axis is time over a 15 s segment of data; *Y*-axis is joystick excursion

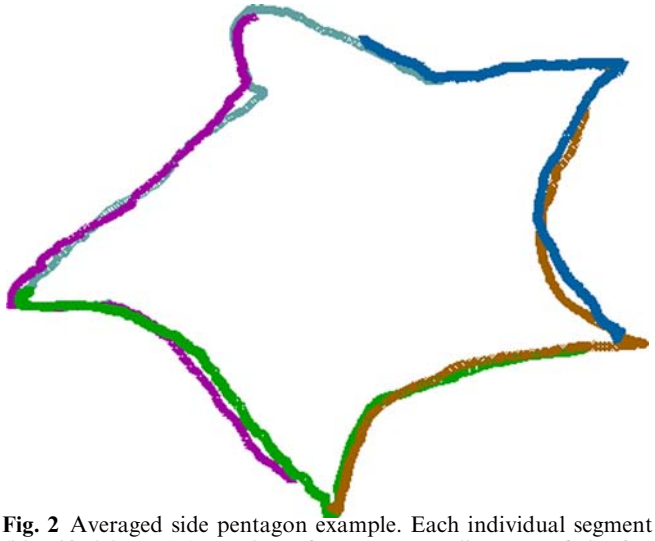

Fig. 2 Averaged side pentagon example. Each individual segment (identified by *color*) consists of 500 ms preceding one of the five corners, to 500 ms after the corner. This representation of each averaged side demonstrates a significant amount of overlap between segments, indicative of accurate corner identification prior to averaging

usually due to the fact that subjects temporarily rotated the pentagon copy for one or two instances. These rotations were apparent from differences in the *X* and *Y* recordings for that pentagon copy. Mismatched sides were excluded from the averages.

Filters were not applied during averaging. However, individual sensors and epochs were screened for exclusion before contributing to the analysis. Inclusion thresholds were determined using the BESA artifact rejection tool. Since the eye-blinks had been identified and excluded already, this step was used to reject excessively noisy sensor channels, and/or epochs. All epochs and sensors with amplitudes over 1.3 pT were excluded from future analyses. Depending upon the shape-copying pace of the subject and the quality of their data, between 3 and 15 iterations of a corner were averaged together for a single corner average, resulting in 14–70 epochs being included in the grand average of all corners.

After averaging, the *XY* data were graphed to determine the quality of each averaged corner (Fig. 2 for an example). Plotting the averaged data demonstrated epochs, which overlapped with surrounding epochs, and rarely included a surrounding corner. In one subject, one corner was inconsistently located relative to the adjacent corners, as identified by side averages, which did not overlap. This corner was left out of all subsequent averaging.

During the flux and dipole mapping portions of the protocol, filters were set to 1 Hz (6 db/oc slope) low cutoff, and 44 Hz (12 db/oc slope) high cutoff. A standard head shape was fit to the sensor positions for each subject based on the fiducial information gathered during the study. This standard head shape is a feature of the BESA software and was used only for flux map viewing and was not used for further computation of dipole locations. Flux appeared as evolving positive and negative topologies on this aligned surface (Fig. 3a). Flux maps were examined for each data point from −500 to +500 ms, noting the evolution and peak of dipolar distributions. Once potential dipoles were identified, the flux image was used to identify relevant sensors by noting the channel numbers of those sensors located over the dipolar distribution (Valaki et al. 2004) (Fig. 3b).

In order to translate dipole coordinates from MEG to the subject's anatomical MRI, it was necessary to have an MRI surface rendering with which to align the data. Renderings were created using BrainVoyager 2000 MRI software (Version 4.9, BrainInnovation, The Netherlands). Surface renderings were made after segmentation and reorientation of each subject's anatomical MRI. Reorientation was performed (rather than spatial warping) in order to place each subject's anatomical study roughly into the Talairach coordinate system (Talairach and Tournoux 1993). The surface points and relative location of the anatomical fiducials, created with a digitizing pen drawn over the scalp before each MEG session, were used to align the surface rendering with the MEG.

Anatomical fiducials (the nasion and the bilateral centers of the acoustic meatus) were identified by hand

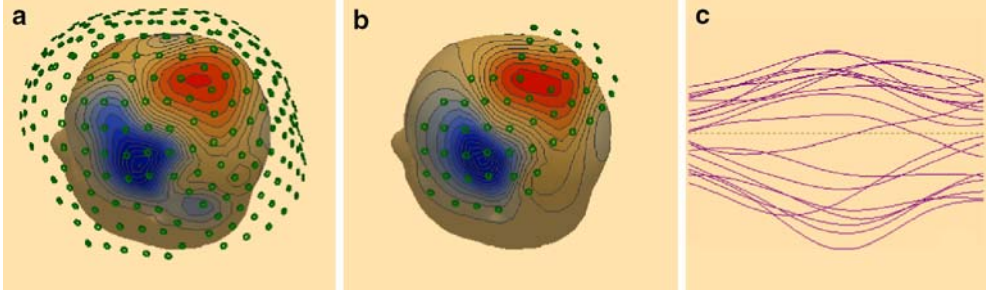

Fig. 3 Dipolar flux map distribution, overlying sensors and respective time traces. **a** shows the flux map distribution of current extrapolated from all 248 sensors and displayed on the standard BESA head shape. **b** shows the flux map distribution of current extrapolated from only those sensors *circled* in **(a)**. **c** shows the resulting waveforms for each sensor in **(b)**. The *X*-axis is time, measuring 30 ms, the *Y*-axis is amplitude, measuring approximately ±10 nAmps, with the *dotted line* = 0

on the MRI. Once entered, the fiducial points of the digitization were moved into position to align the scalp digitization. For closer coordination, the surface points were fit to the scalp rendering using least squares approximation. The mean distance errors were noted after this step and ranged from 1.12 to 2.4 mm. Next, the center of the head (defined as the mid-point between anterior and posterior commissures on the midsagittal plane of the MRI) was submitted as the center sphere location to BESA.

For each potential dipole source identified by the flux maps, only those sensors over the flux map distribution were used for localization (Valaki et al. 2004) (Fig. 3). At least ten sensors were used for localization. On average, 20 (SD ± 6) sensors were used for each of the 116 dipoles reported (also see Table 1). For each potential dipole, a ±20 ms portion of the time-series was selected for analysis, centered on the time point of maximum flux amplitude. The shapes of the overlapping sensor waveforms, which created the flux map distribution were then displayed (Fig. 3c). The entire waveform was included in the localization calculation.

An initial source location was placed by hand, and the residual variance was calculated as the sum of the squared differences between the measured and modeled data over all channels and samples, divided by the total variance of the measured data. Source locations were incrementally relocated using the default settings of the analysis software until the residual variance was minimized. To be considered a potential source, the resulting dipole model had to localize beneath the selected sensors. For each dipole model, the amplitude of the waveform was taken into consideration. If the waveform was complete (included both the onset digression from the mean signal amplitude as well as the return to baseline), lasted longer than 10 ms, and the goodness-of-fit was greater than or equal to 90%, the dipole was accepted. If the dipole showed less than 90% goodness-of-fit, less of the waveform (but at least 10 ms) was used for refitting. If the waveform used for the fit was incomplete, but the partial waveform achieved a 90% goodness-of-fit, the time points that contained the overall waveform were noted, and the best-fit localization analysis was repeated using the expanded range of time points. If the waveform was multi-peaked, individual peaks were analyzed. If there was a shift in location of the dipole between the two peaks great enough to identify two dipoles separated by more than 10 mm, the peak, which included the time point from the flux map was used for dipole localization, and a separate dipole was modeled for the second peak.

When an acceptable waveform was identified, a potential dipole was submitted to BrainVoyager. The final criterion for acceptance of a dipole model was based on physiological plausibility. A dipole was considered physiologically implausible if it was located outside of gray matter or the calculated current was greater than ±25 nAmps. Dipole localization loses accuracy with increasing distance from the sensors (Hillebrand and Barnes 2002). Furthermore, the currents necessary to

Table 1 Grand average dipole results

Location	Number of dipoles	Number of subjects	Number of sensors	|nAmp|	*X*	*Y*	*Z*	Number of dipole attempts	Percentage low fit	Percentage < 10 ms	Percentage phys imp
L Frontal	7	4	19 ± 5	5 ± 2	−35 ± 13	19 ± 15	30 ± 19	22	32	0	36
R Frontal	6	3	15 ± 2	8 ± 3	31 ± 7	27 ± 19	16 ± 21	16	31	0	31
Frontal	13	6	17 ± 4	7 ± 3	na	na	na	38	32	0	34
L Motor	27	8	21 ± 5	8 ± 4	−37 ± 8	−18 ± 8	40 ± 11	76	32	7	26
R Motor	7	3	18 ± 5	7 ± 4	42 ± 12	−13 ± 15	34 ± 11	22	36	5	27
Motor	34	8	20 ± 5	7 ± 4	na	na	na	98	33	6	27
L Parietal	8	6	18 ± 4	5 ± 3	−43 ± 9	−47 ± 13	28 ± 8	39	31	10	38
R Parietal	8	5	19 ± 4	9 ± 5	39 ± 16	−52 ± 9	20 ± 19	22	27	0	36
Parietal	16	8	19 ± 4	7 ± 4	na	na	na	61	30	7	38
L STG	14	6	15 ± 4	11 ± 6	−39 ± 27	−19 ± 10	2 ± 13	34	21	3	35
R STG	10	7	16 ± 3	6 ± 4	47 ± 12	−19 ± 11	6 ± 12	44	32	7	39
STG	24	9	15 ± 3	9 ± 6	na	na	na	78	27	5	37
Visual	29	9	26 ± 6	10 ± 6	−3 ± 14	−78 ± 11	19 ± 13	63	29	2	24

This lists dipoles for a majority of subjects. *STG* refers to the superior temporal gyrus. *L* and *R* are left and right, respectively. Frontal, motor, parietal, and STG without a preceding L or R refer to dipoles localized to *either* side. Number of dipoles refers to the total number of valid dipoles across subjects localized in that region. Number of subjects refers to how many of the ten subjects showed a dipole, which met our criteria within this region. Number of sensors refers to how many sensors were used per localization (mean ± SD). |nAmps| refers to the absolute current of the dipole model in nano-amps (mean ± SD). *X*, *Y*, and *Z* refer to left/right, anterior/posterior, and rostral/caudal dimensions, respectively (mean ± SD across dipoles within that category). Measurements (in mm) are from the origin as in the Talairach system (Talairach and Tournoux 1993). +*X* is to the right, +*Y* is anterior, and +*Z* is rostral. Number of dipole attempts refers to the total number of flux map dipolar distributions used to fit both valid and rejected dipoles. Percentage low-fit refers to the percentage of dipole attempts, which were rejected based on not meeting the criterion of having goodness-of-fit greater than or equal to 90%. Percentage <10 ms refers to the percentage of dipole attempts which were rejected based on not meeting the criterion of at least 10 ms duration. Percentage phys imp refers to the percentage of dipole attempts which were rejected based on physiological implausibility; this category included dipoles with calculated currents greater than 25 |nAmp| and/or those dipoles which localized outside of cortical gray matter

make deep sources detectable are likely to be supra-physiological or representative of one dipole model accounting for data from multiple shallow sources. If the dipole met all the acceptance criteria, the location, orientation, and amplitude were recorded. These steps were repeated for all potential sources as identified by flux maps throughout the averaged data set.

Results

In dipole analyses of the grand averages (all pentagon corners averaged together) within each subject, multiple cortical sources were identified that were prevalent across subjects. Most notably, dipole models meeting our inclusion criteria were localized in the visual cortex, left motor cortex, bilateral frontal cortices, bilateral parietal cortices and bilateral superior temporal gyri (STG) in a majority of subjects (Table 1 and Figs. 4, 5). In addition to these results, data from a limited number of subjects (<4) also localized dipoles to the left lateral occipital cortex, supplementary motor area, bilateral middle temporal gyri, right pre- and post-central sulci, and bilateral insulae.

With regard to the temporal progression of appearance of these dipoles, motor and frontal dipoles were spread evenly across pre-corner and post-corner time points. The majority of visual dipoles, however, were found in the time points following the corners (21 of 29). Conversely, most of the STG dipoles were found in the time points preceding the corners (18 of 25). This trend was more pronounced when looking only at the left STG, in which all 15 appeared prior to the time point used for corner averaging. The temporal extent of these dipoles, in milliseconds, was variable (mean $\pm$ SD): frontal (31 ± 19), left motor (46 ± 30), parietal (29 ± 14), STG (31 ± 17), and visual (27 ± 10).

Discussion

Traditional MEG studies using high numbers of repeated task periods, in which responses are averaged together, demonstrate accurate localization of cortical neural activity. Comparison of MEG-based localization techniques to the gold standard of intraoperative localization is ongoing. A recent study of MEG localization of functional neural tissue with regard to sensory, mo-

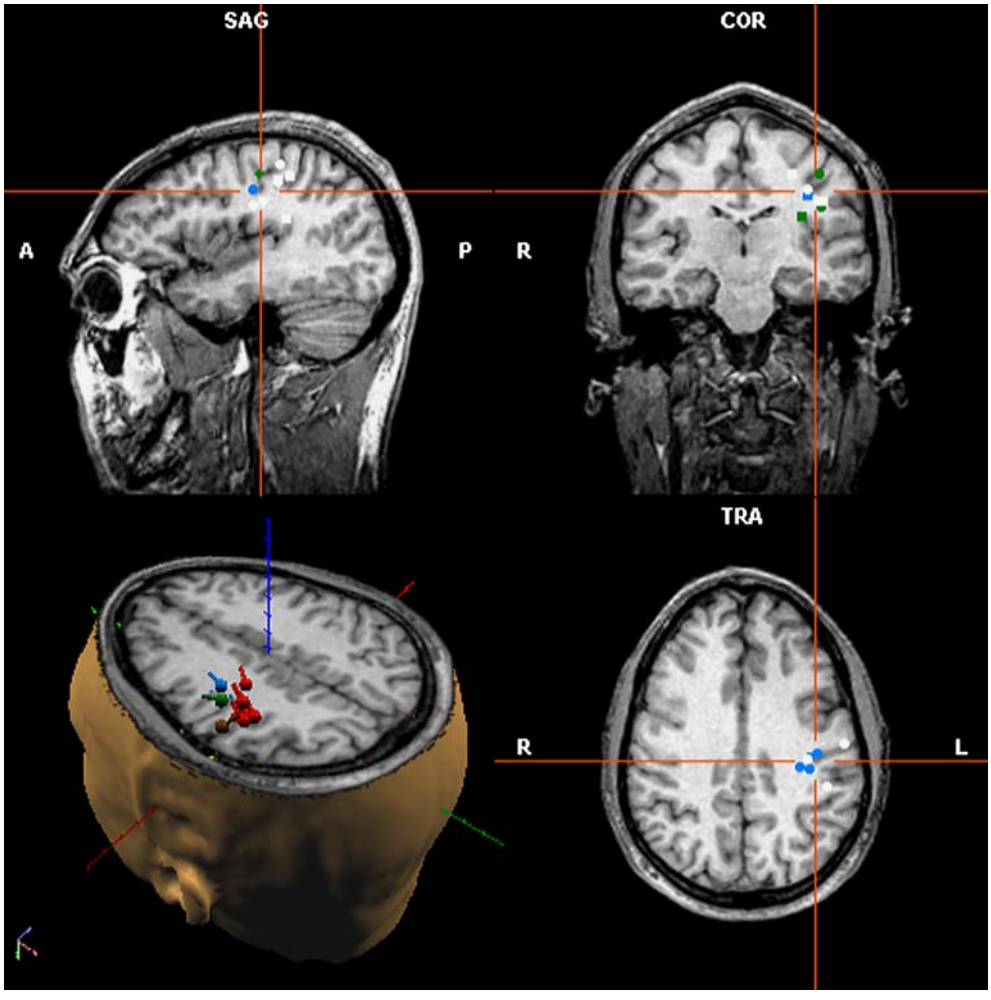

Fig. 4 Dipoles from eight subjects in left motor cortex. Dipoles are localized on a single subject's anatomical MR image using Talairach coordinates. *Upper left panel* is a parasagittal view. *Upper right view* is a coronal section. *Lower right panel* is a transverse section aligned to AC–PC line. *Lower left panel* is a volumetric rendering. Each subject is represented by a *different color*

tor, visual, and language related cortical areas, included 170, 95, 5, and 68 patients, respectively (Ganslandt et al. 2002). The authors stated that stereotaxic correspondence was high for each, with 97% successful MEG based localization for sensory cortex, 90% for motor, 100% for visual, 90% for Broca's area, and 95% for Wernicke's area. Another group has similarly used MEG for pre-operative evaluation of eloquent cortex with positive results (Hund et al. 1997). A recent study found differences between dipole localization and subsequent intraoperative identification of motor activity to average only 5.9 mm (SD of 1.7 mm) in nine subjects (Ganslandt et al. 1997). Another study used a sensorimotor task followed by electrocorticography to demonstrate the accuracy and replicability of MEG localization in motor and sensory cortex (Castillo et al. 2004). These studies involved highly stereotyped movements, repeated multiple times for averaging.

Our work involved continuous motor activity with averages aligned by changes within the joystick output. We identified activity in the left motor cortex for eight of ten subjects. While these equivalent current dipoles probably do not represent *all* left motor cortical activity involved in the task for each subject, the high level of correspondence among subjects suggests that the region may adequately represent cortex utilized in most subjects for performance of the copy task. The usefulness of this approach is supported by the consistent localization of cortical activity across a majority of the ten subjects we studied (Table 1).

In addition to the expected left motor cortical activity, three of ten subjects demonstrated ipsilateral (right hemisphere) motor cortical activity associated with the task at no consistent temporal relationship to the averaged corner. Ipsilateral motor cortical activity has been noted in multiple brain mapping studies including PET (Sadato et al. 1996; Catalan et al. 1998), fMRI (Kim et al. 1993; Rao et al. 1993), and MEG (Huang et al. 2004). It has been speculated that this ipsilateral involvement could be due to anatomical evidence that 10–15% of lateral corticospinal tract fibers remain uncrossed (Kim et al. 1993). It has also been suggested that the ipsilateral activity is due to inhibition of homologous activity in an unmoving limb (Cheyne and Weinberg 1989; Cheyne et al. 1995).

Visual cortical activity was found in nine of ten subjects. The tenth subject showed visual dipole trends, which did not meet our criteria for acceptance. This

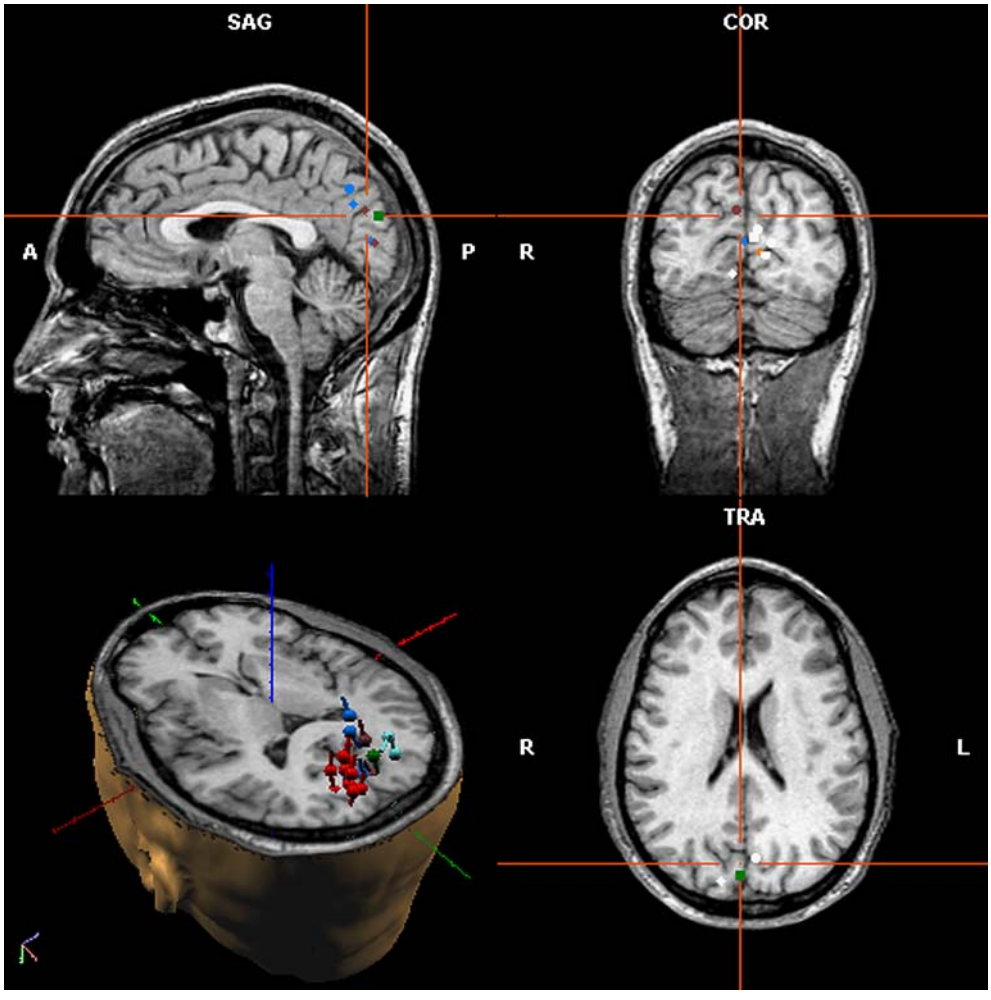

Fig. 5 Dipoles from nine subjects in visual cortex. Dipoles are localized on a single subject's anatomical image using Talairach coordinates. *Upper left panel* is a parasagittal view. *Upper right view* is a coronal section. *Lower right panel* is a transverse section aligned to AC–PC line. *Lower left panel* is a volumetric rendering. Each subject is represented by a *different color*

finding in nine subjects is particularly interesting given that no repeated visual stimulus was presented. A recent study suggested that alpha rhythm is inversely related to the importance of visual stimuli, and that attention may reduce alpha by increasing the exchange of information between parietal and occipital regions (Vanni et al. 1997). These authors hypothesized that the dorsal region of the parieto-occipital sulcus functions to direct parietal activity to a visual object. In this manner, the visual cortex may have been utilized within a network of cortical regions to continually update the motor template in subjects during our copy task. This possibility is supported by the generally dorsal localization of visual activity seen in our subjects (Table 1 and Fig. 5). Furthermore, by the nature of our averaging technique, this visually guided interaction appears to have been regularly related to the corners of each copy segment. However, it must be emphasized that this possible visual cortex referencing demonstrated limited temporal consistency across subjects, although the majority of visual dipoles appeared in the time-span following the corner used for averaging. This suggests that shortly after motor plan execution (in the form of directional change), the dorsal visual cortex was active, which may reflect that a template was referenced for further motor planning.

Lesions of the parietal cortex have been implicated in constructional apraxia. While early work appeared to implicate the right hemisphere in constructional apraxia (Piercy et al. 1960; Benton 1967; Mack and Levine 1981), later studies suggested that both hemispheres may play a role (De Renzi 1982; Gainotti 1985). Our bilateral dipole localizations in the parietal cortices support the latter view. However, the varied locations of dipoles within the parietal cortices provide little additional information.

Numerous hypotheses may explain the activity we identified in the temporal gyri and insulae. These include movement related effects, as well as potential involvement in the comparison of the visual template and motor output. Interpretations of these results remain speculative.

The frontal lobes have been implicated in executive function for many attended tasks (see Roberts et al. 1996; for a review). Working memory comprises one area of extensive research regarding the role of the frontal lobes (Smith and Jonides 1999). More specific to copying shapes, Averbeck et al. (2002, 2003) identified and characterized neural activity in the frontal lobes of non-human primates during copying. These results, along with the extensive working memory and executive function literature, suggest roles for the frontal dipole activity we identified in six of ten subjects during our task.

From the literature, one might expect to find dorsolateral prefrontal cortex (DLPFC) and anterior cingulate gyrus involvement in a demanding working memory and motor planning task such as this (Averbeck et al. 2002, 2003; Brown et al. 2005). While DLPFC dipoles and dipole trends were identified, the former were included in the general category of frontal dipoles due to the wide distribution of hemisphere and location. This lack of consistency across subjects may reflect individual differences in task performance. The perceived paucity of activity in these particular regions likely also reflects our experimental design. DLPFC and anterior cingulate gyrus would be expected to play a role in initial task planning as well as error detection and correction. In considering this experiment, initial planning likely took place during the time-period preceding the start of movement, or, at best, during the initial iterations of the continuous pentagon copying. As many more iterations were performed and used for averaging, it is possible that any specific planning in which DLPFC was recruited was minimized through averaging. Likewise, one would expect a stochastic distribution of performance errors throughout the task. This would also result in minimized (rather than enhanced) anterior cingulate and DLPFC activity after averaging. Furthermore, inconsistent corners, eye-blinks, and saccades were all excluded from analysis; each of which may be related to errors, perceived errors or error correction, thus further reducing the likelihood of identifying activity within error associated cortical regions.

Given earlier work in fMRI using this task (Lewis et al. 2003) we anticipated identifying cerebellar activity. While we identified potential dipole trends within the cerebellum, no dipoles achieved our acceptance criteria in this region. This may have been due to the distance of the cerebellum from the MEG sensors and/or less focal activity in the cerebellum that was more difficult to model successfully.

Our results indicate that cortical regions involved in this task were consistently active with regard to the motor output such that we could create averages and localize physiologically plausible dipoles using a continuous behavioral measure. We did not find precise consistency across subjects in the relationship of dipoles to their temporal location within the cornering trajectory (e.g. all visual dipoles 50 ms after the corner in most subjects). This may be due to individual differences in task performance. However, relative trends were observed in identification of visual cortical dipoles following the corners, and insulae/STG activity preceding the corners. Taken in the context of continuous copying, STG/insulae activity before the upcoming corners preceded the change in trajectory, while visual cortical activity tended to follow the change in trajectory. The existence of consistent visual dipoles in nine of ten subjects absent eye blinks, eye movements, or changes in the visual environment, indicates that visual cortex was consistently active within subjects with respect to the motor output of a change in trajectory. This finding suggests that the visual cortex may be in continued interaction with other cortical regions in order to complete the copy task. This hypothesis is supported by the temporal relationship between each corner and the visual dipoles generally located in the dorsal regions of the parieto-occipital sulcus, which implies that the dorsal stream components of later visual processing were con-

sistently under load following directional changes in the motor output.

Acknowledgments This work was supported by the MIND Institute (Albuquerque, NM), the U.S. Department of Veterans Affairs, and the American Legion Brain Sciences Chair.

References

Averbeck BB, Chafee MV, Crowe DA, Georgopoulos AP (2002) Parallel processing of serial movements in prefrontal cortex. Proc Natl Acad Sci USA 99:13172–13177

Averbeck BB, Chafee MV, Crowe DA, Georgopoulos AP (2003) Neural activity in prefrontal cortex during copying geometrical shapes. I. Single cells encode shape, sequence, and metric parameters. Exp Brain Res 150:127–141

Behrmann M, Winocur G, Moscovitch M (1992) Dissociation between mental imagery and object recognition in a brain-damaged patient. Nature 359:636–637

Benton A (1967) Constructional apraxia and the minor hemisphere. Confin Neurol 29:1–16

Bernstein N (1923) The problem of the interrelation of co-ordination and localization. In: Whiting HTA (ed) Human motor actions Bernstein reassessed. North-Holland, 1984, New York, pp 75–119

Brown JW, Braver TS (2005) Learned predictions of error likelihood in the anterior cingulate cortex. Science 307:1118–1121

Castillo EM, Simos PG, Wheless JW, Baumgartner JE, Breier JI, Billingsley RL, Sarkari S, Fitzgerald ME, Papanicolaou AC (2004) Integrating sensory and motor mapping in a comprehensive MEG protocol: clinical validity and replicability. Neuroimage 21:973–983

Catalan MJ, Honda M, Weeks RA, Cohen LG, Hallett M (1998) The functional neuroanatomy of simple and complex sequential finger movements: a PET study. Brain 121:253–264

Cheyne D, Weinberg H (1989) Neuromagnetic fields accompanying unilateral finger movements: pre-movement and movement-evoked fields. Exp Brain Res 78:604–612

Cheyne D, Weinberg H, Gaetz W, Jantzen KJ (1995) Motor cortex activity and predicting side of movement: neural network and dipole analysis of pre-movement magnetic fields. Neurosci Lett 188:81–84

De Renzi E (1982) Disorders of space exploration and cognition. Wiley, Baffins Lane

Folstein MF, Folstein SE, McHugh PR (1975) ''Mini-mental state''. A practical method for grading the cognitive state of patients for the clinician. J Psychiatr Res 12:189–198

Gainotti G (1985) Constructional apraxia Handbook of clinical neurology. Elsevier, Amsterdam, pp 491–506

Ganslandt O, Steinmeier R, Kober H, Vieth J, Kassubek J, Romstock J, Strauss C, Fahlbusch R (1997) Magnetic source imaging combined with image-guided frameless stereotaxy: a new method in surgery around the motor strip. Neurosurgery 41:621–627; discussion 627–628

Ganslandt O, Fahlbusch R, Kober H, Gralla J, Nimsky C (2002) Use of magnetoencephalography and functional neuronavigation in planning and surgery of brain tumors. Nervenarzt 73:155–161

Georgopoulos AP (2002) Behavioral and neural aspects of motor topology: following Bernstein's thread. In: Latash ML (ed) Progress in motor control, vol 2: structure-function relations in voluntary movements, Human Kinetics, Champaign, IL, pp 1–12

Hillebrand A, Barnes GR (2002) A quantitative assessment of the sensitivity of whole-head MEG to activity in the adult human cortex. NeuroImage 16:638–650

Huang MX, Harrington DL, Paulson KM, Weisend MP, Lee RR (2004) Temporal dynamics of ipsilateral and contralateral motor activity during voluntary finger movement. Hum Brain Mapp 23:26–39

Hund M, Rezai AR, Kronberg E, Cappell J, Zonenshayn M, Ribary U, Kelly PJ, Llinas R (1997) Magnetoencephalographic mapping: basic of a new functional risk profile in the selection of patients with cortical brain lesions. Neurosurgery 40:936–942; discussion 942–943

Kim SG, Ashe J, Hendrich K, Ellermann JM, Merkle H, Ugurbil K, Georgopoulos AP (1993) Functional magnetic resonance imaging of motor cortex: hemispheric asymmetry and handedness. Science 261:615–617

Kleist K (1934) Gehirnpathologie. Barth, Liepzig

Leuthold AC (2003) Subtraction of heart artifact from MEG data: the matched filter revisited. Society for Neuroscience Abstracts 863.15

Lewis SM, Jerde TA, Tzagarakis C, Georgopoulos MA, Tsekos N, Amirikian B, Kim SG, Ugurbil K, Georgopoulos AP (2003) Cerebellar activation during copying geometrical shapes. J Neurophysiol 90:3874–3887

Mack JL, Levine RN (1981) The basis of visual constructional disability in patients with unilateral cerebellar lesions. Cortex 17:515–532

Piercy M, Hecaen H, Ajuriaguerra J (1960) Constructional apraxia associated with unilateral cerebral lesions. Left and right sided cases compared. Brain 83:225–242

Rao SM, Binder JR, Bandettini PA, Hammeke TA, Yetkin FZ, Jesmanowicz A, Lisk LM, Morris GL, Mueller WM, Estkowski LD (1993) Functional magnetic resonance imaging of complex human movements. Neurology 43:2311–2318

Roberts AC, Robbins TW, Weiskrantz L (1996) Executive and cognitive functions of the prefrontal cortex. R Soc Phil Trans Biol Sci Ser B 351:1397–1527

Sadato N, Campbell G, Ibanez V, Deiber M, Hallett M (1996) Complexity affects regional cerebral blood flow change during sequential finger movements. J Neurosci 16:2691–2700

Smith EE, Jonides J (1999) Storage and executive processes in the frontal lobes. Science 283:1657–1661

Talairach J, Tournoux P (1993) Referentially oriented cerebral MRI anatomy. Georg Thieme Verlag, New York

Valaki CE, Maestu F, Simos PG, Zhang W, Fernandez A, Amo CM, Ortiz TM, Papanicolaou AC (2004) Cortical organization for receptive language functions in Chinese, English, and Spanish: a cross-linguistic MEG study. Neuropsychologia 42:967–979

Vanni S, Revonsuo A, Hari R (1997) Modulation of the parieto-occipital alpha rhythm during object detection. J Neurosci 17:7141–7147